Fluorescence and absorption by a two-level atom in a bichromatic field with one strong and one weak component

Z. Ficek[1] and H. S. Freedhoff[2,*]
[1]Department of Physics, The University of Queensland, Brisbane, Queensland 4072, Australia
and [2]Department of Physics, University of Toronto, Toronto, Ontario, Canada M5S 1A7
(Received 29 June 1995)

We analyze the fluorescence and absorption spectra of a two-level atom driven by a bichromatic field with frequencies ω_1 and ω_2, separated by $\omega_2-\omega_1=2\delta$, and Rabi frequencies (at resonance) $2\Omega_1$ and $2\Omega_2$ such that their ratio $\alpha=\Omega_2/\Omega_1<1$. We focus on the case of ω_1 close to the atomic frequency ω_0 and ω_2 near the Rabi sideband frequency $\omega_1+2\Omega_1$; the detunings are denoted by $\Delta_1=\omega_0-\omega_1$ and $\Delta_2=\omega_1+2\Omega_1-\omega_2$. We find that the spectra depend critically on the detuning Δ_2: For large Δ_2, the fluorescence spectrum consists of the well known Mollow triplet, centered at ω_1; for smaller (but nonzero) Δ_2, the spectrum is composed of a triplet at ω_1 together with doublets near the sideband frequencies $\omega_1\pm2\Omega_1$. However, when $\Delta_2=0$ (and $\alpha\ll1$), the spectrum consists of a doublet centered at ω_1 and triplets at $\omega_1\pm2\Omega_1$: there is then no fluorescence at ω_1. As α increases, additional triplet structures appear in the spectrum at frequencies $\omega_1\pm2n\Omega_1$ with intensities proportional to $\alpha^{2(n-1)}$, $n>1$, and a line reappears at ω_1, with intensity proportional to α^4. The absorption by the system of a weak probe beam is also strongly dependent on the detuning, and the spectrum is composed of emission-dispersion-absorption features located near ω_1 and $\omega_1\pm2n\Omega_1$. An analysis in the dressed-atom picture is presented which explains the physical origin of all these features, in both fluorescence and absorption. [S1050-2947(96)06305-6]

PACS number(s): 42.50.Hz, 32.80.−t

I. INTRODUCTION

The resonance fluorescence and absorption of a weak probe beam by a strongly driven atom has been studied extensively for many years. Initially, these studies involved an intense monochromatic driving field. Their most dramatic results included the prediction and observation of the ''Mollow triplet'' for the fluorescence spectrum [1,2], consisting of a central component at frequency ω_L and sidebands at $\omega_L\pm2\Omega$, where ω_L is the driving frequency and 2Ω the Rabi frequency of the laser field.

The fluorescence and probe absorption by an atom in a strong bichromatic driving field has also been studied extensively, both theoretically and experimentally [3–23]. The interest stems mostly from the observation that the bichromatic nature of the driving field leads to a number of novel features which are not present in the monochromatic case. For example, the transient fluorescence intensity exhibits an interesting dependence on the initial phase difference between the driving field components, and resonances at subharmonics of the Rabi frequency as well as at the components' beat frequency [10,17].

In this paper, we concentrate on the spectra corresponding to fluorescence and probe absorption in a bichromatic driving field. The fluorescence spectrum has been calculated for equal-amplitude field components symmetrically detuned from the atomic frequency ω_0 [5,9,11–13], equal-amplitude components asymmetrically detuned [14,16], and components having unequal amplitudes [16]. The spectra consist of a central component at the average driving frequency $\omega_s=(\omega_1+\omega_2)/2$ and a series of sidebands separated by integer multiples of δ, half the separation frequency. When the driving components are symmetrically detuned from ω_0 and have equal Rabi frequencies 2Ω, the peak separations are independent of 2Ω, but their number increases with increasing 2Ω, and their widths and amplitudes oscillate. For unequal Rabi frequencies and/or asymmetrically detuned driving field components, the central component of the spectrum and the peaks separated from it by even multiples of δ split into doublets [16], whose positions and splittings vary as a function of the detunings and Rabi frequencies. This splitting has recently been observed experimentally [22]. A physical understanding of these effects is achieved by using a dressed-atom description of the atom-field system [23,24]. In this approach, eigenstates of the atom-plus-driving-field serve as the basis states for the system. In the case of bichromatic excitation, the energy spectrum corresponds to manifolds of states separated by ω_s; within each manifold, the states are separated by integer multiples of δ [12]. The multipeak spectra are interpreted as the result of transitions between the dressed states of neighboring manifolds.

The multipeak sidebands in the fluorescence spectrum are features which arise in a bichromatic driving field whose components have equal or almost equal Rabi frequencies. Although most of the theoretical work to date has been concerned only with equal Rabi frequencies (equivalent to an amplitude-modulated field with the resonant carrier suppressed), there are also (different) novel features which occur for the case of one strong and one weak component of the bichromatic field. There have now been several experiments which examine the subharmonic resonances [10], the transient behavior of the atoms [17], and the Autler-Townes spectrum [20] in this limit. The remarkable features of these

*Permanent address: Department of Physics and Astronomy, York University, Toronto, Ontario, Canada M3J 1P3.

experiments are the multiphoton resonances at subharmonics of the Rabi frequencies [6–8], the phase-dependent atomic dynamics even if the interaction begins with atoms in their ground states [17], and a four-peak structure of the Autler-Townes spectrum [20]. These effects associated with unequal driving-field intensities suggest the possibility of interesting modifications of the spectral properties of the fluorescence field as well.

One purpose of this paper is to present a detailed analysis of the fluorescence spectrum in the limit of one strong and one weak component of the bichromatic field. As we will see below, the spectrum is qualitatively different from both the Mollow triplet observed for a monochromatic driving field and the multipeak spectrum characteristic of a bichromatic driving field with equal component intensities. In particular, the components of the (original) Mollow triplet are each split into either a triplet or a doublet depending on the detuning Δ_2 of the weak field component from the Rabi sideband induced by the strong field. In the special case of $\Delta_2=0$ and $\alpha\ll 1$, the component at ω_1 of the fluorescence spectrum completely disappears. These features are explained by the effect on the ω_1 dressed states of the ω_2 field component and by the spontaneous emission transition rates between the resultant doubly dressed states. We emphasize too the following significant difference: For a bichromatic driving field with one strong and one weak component the spectral features are centered about the frequency ω_1 of the strong component and its Rabi sidebands, whereas for a bichromatic field with (nearly) equal amplitudes, they are centered about the mean frequency ω_s of the field components and $\omega_s\pm m\delta$.

In addition to modifications in the fluorescence spectrum, one can also observe changes in the absorption spectrum of a probe beam that interacts with a bichromatically driven atom. The probe and bichromatic fields can be tuned to the same atomic transition, or alternatively, the probe can be tuned to a transition sharing one common level with the bichromatically driven transition. In the first case a Mollow type [25], whereas in the second case an Autler-Townes [26] type spectrum is monitored. Recent studies of the Mollow-type absorption spectrum with a bichromatic driving field of equal amplitudes have led to the prediction of new regions of frequency where the probe beam can be amplified. Moreover, when ω_s is detuned from ω_0 and/or the amplitudes of the field components are slightly different, the central component of the absorption spectrum and the even sidebands split into emission-absorption doublets, whereas the odd sidebands remain dispersionlike [16]. This splitting has recently been observed experimentally in the Autler-Townes spectrum in both a detuned bichromatic field [22], and a resonant bichromatic field with unequal component amplitudes [20]. In this paper we calculate the absorption spectrum in the limit of one strong and one weak component of the driving field; we restrict the calculations to the (Mollow-type) absorption spectrum. As in the case of fluorescence, these spectra are again very different from those obtained previously. We find that two different types of spectra can be observed, depending on the detuning Δ_2. For $\Delta_2\neq 0$ the spectrum exhibits triplet emission-dispersion-absorption structures about ω_1 and $\omega_1\pm 2\Omega_1$. In contrast, for $\Delta_2=0$, the central component at ω_1 is suppressed. A simple physical interpretation of these results is given in terms of the dressed states of the system. Positions, intensities, and widths of the spectral features are determined from the energies, populations, and transition rates associated with the dressed-atom states.

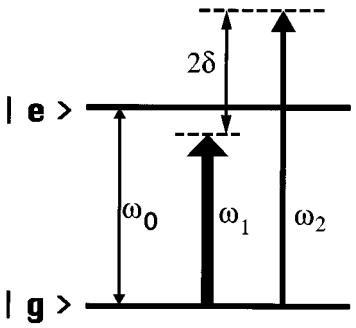

FIG. 1. System composed of a two-level atom driven by a bichromatic field whose components have different intensities.

The paper is organized as follows: In Sec. II we describe in detail our model and discuss the methods we use to calculate the fluorescence and absorption spectra and to explain their features. In Sec. III we calculate the spectral expressions in the framework of a classical driving field. The calculations are based on a Floquet method using the optical Bloch equations and continued fraction techniques [16]. In Sec. IV we present a quantum dressed-atom model of the system and calculate analytically the fluorescence and absorption spectra. We analyze in detail intensities, widths and positions of the spectral features and compare them with the numerical results presented in Sec. III. Finally, in Sec. V, we summarize our results.

II. THE SYSTEM

We consider a two-level atom with ground state $|g\rangle$, excited state $|e\rangle$, transition frequency ω_0 and dipole transition moment $\vec{\mu}$. The atom is driven by a bichromatic field (Fig. 1) with frequency components ω_1 and ω_2 separated by $\omega_2-\omega_1\equiv 2\delta$ and with detunings

$$\Delta_1=\omega_0-\omega_1, \quad \Delta_2=\omega_1+2\Omega_1-\omega_2. \tag{2.1}$$

The atom is also coupled to all other modes of the electromagnetic field, which are assumed to be initially in their vacuum state. This coupling leads to spontaneous emission with a rate given by the Einstein A coefficient.

The time evolution of the atomic system can be described by the reduced atomic density operator ϱ, which in the Schrödinger picture obeys the master equation [27]

$$\frac{\partial\varrho}{\partial t}=-\frac{i}{\hbar}[H,\varrho]-\frac{1}{2}\Gamma(S^+S^-\varrho+\varrho S^+S^--2S^-\varrho S^+), \tag{2.2}$$

where $S^+=|e\rangle\langle g|$ and $S^-=|g\rangle\langle e|$ are the usual raising and lowering atomic operators and Γ is the radiative damping constant, $\Gamma=A$. The Hamiltonian H is composed of two terms,

$$H=H_0+V_L, \tag{2.3}$$

where

$$H_0=\hbar\omega_0 S^z, \tag{2.4}$$

is the unperturbed atomic Hamiltonian, with S^z the atomic inversion $\frac{1}{2}(|e\rangle\langle e|-|g\rangle\langle g|)$.

The second term in Eq. (2.3) describes the coupling between the driving field and the atom. If we treat the driving field classically, the interaction Hamiltonian V_L (in the rotating-wave approximation) may be written as

$$V_L=\hbar[\Omega_1 S^+\exp(-i\omega_1 t)+\Omega_2 S^+\exp(-i\omega_2 t)+\text{H.c.}], \tag{2.5}$$

where

$$2\Omega_{\frac{1}{2}}=\vec{\mu}\cdot\vec{E}_{\frac{1}{2}}/\hbar, \tag{2.6}$$

are the Rabi frequencies (at resonance) associated with the components of the driving field at frequencies $\omega_{\frac{1}{2}}$. If we use a fully quantum-mechanical description of the system, the effective Hamiltonian (2.3) (in the rotating-wave approximation) takes the form

$$H=H_0'+V_L', \tag{2.7}$$

where

$$H_0'=\hbar\omega_0 S^z+\hbar\omega_1 a_1^+ a_1+\hbar\omega_2 a_2^+ a_2 \tag{2.8}$$

is the Hamiltonian of the uncoupled atom and field,

$$V_L'=\hbar g_1(a_1^+ S^-+S^+ a_1)+\hbar g_2(a_2^+ S^-+S^+ a_2) \tag{2.9}$$

is the atom-field interaction, g is the atom-field coupling constant (equal to the one-photon Rabi frequency), and $a_{1,2}$ ($a_{1,2}^+$) are the annihilation (creation) operators for the driving field modes. In the classical description of the process, the basis states for the system are simply the atomic states $|g\rangle$ and $|e\rangle$. For the quantum treatment, the basis states are product states $|j\rangle|N,M\rangle$ involving products of atomic $|j\rangle$ ($j=g,e$) and driving field ($|N,M\rangle$) states, where N and M denote the number of photons in modes 1 and 2, respectively. These states are the eigenstates of the uncoupled atom and field Hamiltonian (2.8).

In the classical treatment, the term V_L in the Hamiltonian (2.3) is periodic in time, with separation frequency 2δ. The periodicity of the problem makes it advantageous to analyze the system in terms of Floquet states of the atom. In Sec. III, we present in detail Floquet's theorem [28] adapted to the case of a bichromatic field and derive expressions for the fluorescence and absorption spectra in terms of the Floquet states.

In Sec. IV, in the quantum treatment of the problem, the interaction (2.9) is first diagonalized to obtain the dressed states of the atom-field system. We then calculate the fluorescence and absorption spectra in terms of transitions between these dressed-states. The quantum description allows us to obtain both a physical understanding of the process and analytical expressions for the spectra. We find that there is good quantitative agreement between these analytical expressions and those obtained by the full numerical calculations of Sec. III.

III. FLUORESCENCE AND ABSORPTION SPECTRA: A CONTINUED-FRACTION APPROACH

A. Optical Bloch equations

We now consider the fluorescence and absorption spectra of a two-level atom driven by a bichromatic classical field. The spectra were calculated in Refs. [14,16] for equal and nearly equal amplitudes of the two field components, both by a numerical continued-fraction method and (for nearly equal amplitudes) by an analytical perturbation theory method in the dressed-atom basis. In this paper, we focus on the case of one strong and one weak component of the driving field which, as we shall see later, produces dramatically different spectra. A full discussion of the method used to calculate the spectra is given in our basic paper, Ref. [16]. In the interest of brevity, only the key formulas will be given here.

The master equation (2.2) with the Hamiltonian (2.3) leads to a closed set of three equations of motion for the expectation values of the atomic operators (optical Bloch equations), which in a frame oscillating with the frequency ω_s, can be written as

$$\begin{aligned}
\langle\dot{\tilde{S}}^-(t)\rangle&=-\left(\frac{1}{2}\Gamma+i\Delta\right)\langle\tilde{S}^-(t)\rangle\\
&\quad+2(\Omega_1 e^{i\delta t}+\Omega_2 e^{-i\delta t})\langle S^z(t)\rangle,\\
\langle\dot{\tilde{S}}^+(t)\rangle&=-\left(\frac{1}{2}\Gamma-i\Delta\right)\langle\tilde{S}^+(t)\rangle\\
&\quad+2(\Omega_1 e^{-i\delta t}+\Omega_2 e^{i\delta t})\langle S^z(t)\rangle,\\
\langle\dot{S}^z(t)\rangle&=-\frac{1}{2}\Gamma-\Gamma\langle S^z(t)\rangle-(\Omega_1 e^{-i\delta t}+\Omega_2 e^{i\delta t})\langle\tilde{S}^-(t)\rangle\\
&\quad-(\Omega_1 e^{i\delta t}+\Omega_2 e^{-i\delta t})\langle\tilde{S}^+(t)\rangle,
\end{aligned} \tag{3.1}$$

where

$$\langle\tilde{S}^{\pm}(t)\rangle=\pm i\langle S^{\pm}\rangle\exp(\mp i\omega_s t), \tag{3.2}$$

are slowly varying parts of the atomic operators,

$$\Delta=\omega_0-\omega_s \tag{3.3}$$

is the detuning between the atomic transition frequency and the average frequency of the driving field components, and δ is half the separation frequency.

In order to solve the system of equations (3.1), we decompose the components $\langle\tilde{S}^-(t)\rangle$, $\langle\tilde{S}^+(t)\rangle$, and $\langle S^z(t)\rangle$ into amplitudes that oscillate at frequency δ and its harmonics. This decomposition is given by the relation

$$X_i(t)=\sum_{l=-\infty}^{+\infty}X_i^{(l)}(t)\exp(il\delta t),\quad i=1,2,3, \tag{3.4}$$

where $X_i(t)$ are components of the vector $\vec{X}(t)=(\langle\tilde{S}^-(t)\rangle,\langle\tilde{S}^+(t)\rangle,\langle S^z(t)\rangle)$. On substituting (3.4) into (3.1) and taking the Laplace transform

$$X_i^{(l)}(z)=\int_0^{\infty}\exp(-zt)X_i^{(l)}(t)\,dt, \tag{3.5}$$

of the slowly varying amplitudes $X_i^{(l)}(t)$, we find the transforms $X_i^{(l)}(z)$ satisfy a vector recurrence relation

$$A_l\vec{X}^{(l-1)}(z)+(B_l+z_lI)\vec{X}^{(l)}(z)+C_l\vec{X}^{(l+1)}(z)=\vec{X}^{(l)}(0), \tag{3.6}$$

where $z_l=z+il\delta$, $\vec{X}^{(l)}$ are column vectors

$$\vec{X}^{(l)}(z)=\begin{pmatrix} X_1^{(l)}(z)\\ X_2^{(l)}(z)\\ X_3^{(l)}(z)\end{pmatrix},\quad \vec{X}^{(l)}(0)=\begin{pmatrix} X_1^{(l)}(0)\\ X_2^{(l)}(0)\\ X_3^{(l)}(0)-\dfrac{\Gamma}{2z}\,\delta_{l,0}\end{pmatrix}, \tag{3.7}$$

and A_l, B_l, and C_l are matrices:

$$A_l=\begin{pmatrix} 0 & 0 & -2\Omega_1\\ 0 & 0 & -2\Omega_2\\ \Omega_2 & \Omega_1 & 0\end{pmatrix}, \tag{3.8}$$

$$B_l=\begin{pmatrix} \dfrac{1}{2}\Gamma+i\delta & 0 & 0\\ 0 & \dfrac{1}{2}\Gamma-i\delta & 0\\ 0 & 0 & \Gamma\end{pmatrix}, \tag{3.9}$$

$$C_l=\begin{pmatrix} 0 & 0 & -2\Omega_2\\ 0 & 0 & -2\Omega_1\\ \Omega_1 & \Omega_2 & 0\end{pmatrix}. \tag{3.10}$$

We solve Eq. (3.6) numerically by a continued-fraction approach using a truncated basis of harmonic amplitudes. The validity of the truncation is ensured by requiring that $X_i^{(l)}(z)$ not change as the number of harmonics increases by one. Equation (3.6) is valid for arbitrary values of Ω_1, Ω_2, Δ_1, Δ_2, and δ, and all our numerical calculations are based on this exact equation.

B. Fluorescence spectrum

The steady-state fluorescence spectrum is given by the Fourier transform of the two-time correlation function of the atomic operators

$$S(\omega)=u(\vec{r})\mathrm{Re}\int_0^\infty d\tau\,\lim_{t\to\infty}\langle\tilde{S}^+(t)\tilde{S}^-(t+\tau)\rangle e^{i(\omega-\omega_s)\tau}, \tag{3.11}$$

where $u(\vec{r})$ is a normalization constant containing geometric and atomic factors [16,27]. From the quantum regression theorem [29], it is well known that for $\tau>0$ the two-time average $\langle\tilde{S}^+(t)\tilde{S}^-(t+\tau)\rangle$ satisfies the same equation of motion as the one-time average $\langle\tilde{S}^-(\tau)\rangle$. It is not difficult to show that the optical Bloch equations (3.1) for the two-time averages lead to equations of the same form as (3.6), but with the components $X_i^{(l)}(t)$ replaced by

$$\begin{aligned} X_1^{(l)}(t)&\to Y_1^{(l)}(\tau)=\langle\tilde{S}^+(t)\tilde{S}^-(t+\tau)\rangle,\\ X_2^{(l)}(t)&\to Y_2^{(l)}(\tau)=\langle\tilde{S}^+(t)\tilde{S}^+(t+\tau)\rangle,\\ X_3^{(l)}(t)&\to Y_3^{(l)}(\tau)=\langle\tilde{S}^+(t)S^z(t+\tau)\rangle,\end{aligned} \tag{3.12}$$

and the $\vec{X}^{(l)}(0)$ vector replaced by

$$\vec{X}^{(l)}(0)\to\vec{Y}^{(l)}(0)=\begin{pmatrix} X_3^{(l)}(t)\\ 0\\ -\dfrac{1}{2}X_2^{(l)}(t)-\dfrac{\Gamma}{2z}X_2(t)\,\delta_{l,0}\end{pmatrix}. \tag{3.13}$$

The spectrum (3.11) contains an incoherent as well as a coherent part of the field scattered by the atom. Introducing the fluctuation operators

$$\Delta\tilde{S}^\pm(t)=\tilde{S}^\pm(t)-\langle\tilde{S}^\pm(t)\rangle, \tag{3.14}$$

we can write the atomic correlation function appearing in Eq. (3.11) as

$$\begin{aligned}\langle\tilde{S}^+(t)\tilde{S}^-(t+\tau)\rangle=&\langle\Delta\tilde{S}^+(t)\Delta\tilde{S}^-(t+\tau)\rangle\\ &+\langle\tilde{S}^+(t)\rangle\langle\tilde{S}^-(t+\tau)\rangle,\end{aligned} \tag{3.15}$$

where the first term on the right-hand side represents the incoherent part of the field, while the second represents the field scattered coherently by the atom. The incoherent part $S_{in}(\omega)$ of the spectrum can then be calculated by subtracting out the coherent part from the total scattered field

$$\begin{aligned}S_{in}(\omega)=u(\vec{r})\mathrm{Re}\int_0^\infty d\tau e^{i(\omega-\omega_s)\tau}[&\langle\tilde{S}^+(t)\tilde{S}^-(t+\tau)\rangle\\ &-\langle\tilde{S}^+(t)\rangle\langle\tilde{S}^-(t+\tau)\rangle].\end{aligned} \tag{3.16}$$

Introducing the Laplace transform, we express the incoherent fluorescence spectrum in terms of the components of the $\vec{Y}^{(l)}(z)$ and $\vec{X}^{(l)}(t)$ vectors as

$$S_{in}(\omega)=u(\vec{r})\mathrm{Re}\;G(z)\big|_{z=-i\nu}, \tag{3.17}$$

where $\nu=(\omega-\omega_s)/\Gamma$, and

$$G(z)=\lim_{t\to\infty}(Y_1^{(0)}(z)-X_1(t)X_2(t)). \tag{3.18}$$

The fluorescence spectrum can be plotted from Eq. (3.17) with the components $Y_1^{(0)}(z)$ and $X_i^{(l)}(t)$ found from the recursion relation (3.6). We plot the incoherent fluorescence spectra for the case of $\omega_1=\omega_0$ ($\Delta_1=0$),[1] while ω_2 is tuned close to $\omega_1+2\Omega_1$. In Fig. 2 the spectrum is shown for $2\Omega_1=50\Gamma$, $\omega_1=\omega_0$, $\alpha=\Omega_2/\Omega_1=0.1$ and different values of Δ_2. For large Δ_2, the spectrum shows the well known Mollow triplet [1]. For small but nonzero Δ_2, the spectrum exhibits a triplet at the central frequency, with components at $\omega=\{\omega_1$ and $\omega_1\pm2\Omega_2\}$, and doublets at $\omega=\{\omega_2$ and $\omega_2+2\Omega_2\}$

[1]The intensity in the coherently scattered field is proportional to $(\Gamma/2\Omega)^2$, and is completely negligible, both in our calculations and experimentally (see, e.g., Wu *et al.* [2]).

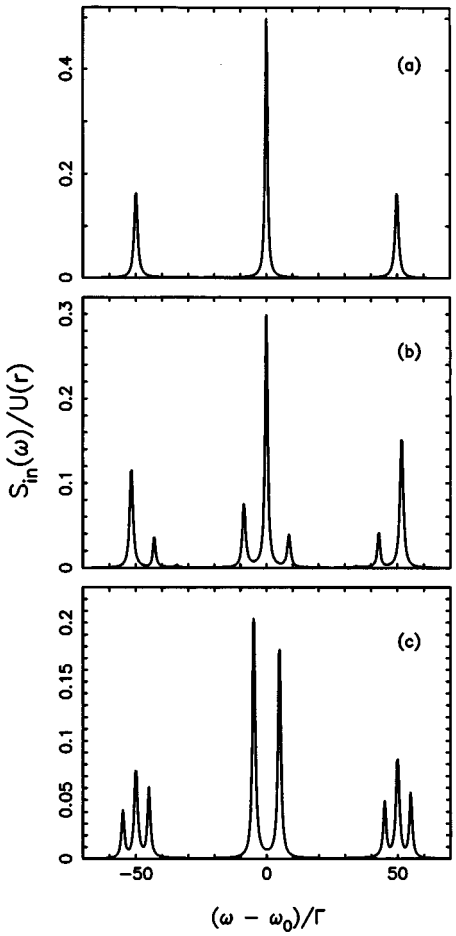

FIG. 2. The fluorescence spectrum for $\omega_1=\omega_0$, $2\Omega_1=50\Gamma$, $\alpha=\Omega_2/\Omega_1=0.2$ and different Δ_2: (a) $\Delta_2\gg 50\Gamma$, (b) $\Delta_2=7\Gamma$, (c) $\Delta_2=0$.

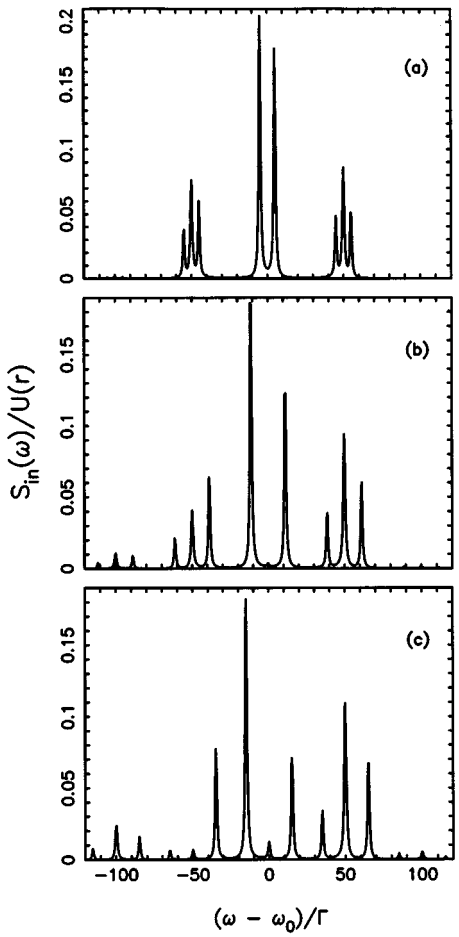

FIG. 3. The fluorescence spectrum for $\omega_1=\omega_0$, $2\Omega_1=50\Gamma$, $\Delta_2=0$ and different α: (a) $\alpha=0.2$, (b) $\alpha=0.4$, (c) $\alpha=0.6$.

and $\omega=\{2\omega_1-\omega_2$ and $2\omega_1-\omega_2-2\Omega_2\}$. A quite different situation develops when Δ_2 is exactly zero: In this case the incoherent central peak at ω_1 is also suppressed (leaving behind a doublet, at $\omega_1\pm 2\Omega_2$),[2] and additional peaks emerge at $\omega=\omega_1+2\Omega_1-2\Omega_2$ and $\omega=\omega_1-2\Omega_1+2\Omega_2$. The spectrum then consists of a doublet near ω_1 and triplets centered at $\omega_1\pm 2\Omega_1$.

When we increase the intensity of the weak component (i.e., α), the peak at ω_1 reemerges. Moreover, additional sidebands (triplets) appear, centered about $\omega_1\pm 4\Omega_1$. This is shown in Fig. 3, where we plot $S_{in}(\omega)$ for $\Delta_1=\Delta_2\equiv 0$, $2\Omega_1=50\Gamma$, and different α. For small α the spectrum exhibits two peaks near ω_1 and triplets centered about $\omega_1\pm 2\Omega_1$. As α increases, additional triplets emerge at $\omega_1\pm 4\Omega_1$. For still larger α ($\alpha=0.6$), the peak at ω_1 reemerges, but with an amplitude significantly smaller than the amplitudes of the remaining peaks. It should be noted that the central peak reappears in the spectrum only for α significantly larger than that required for appearance of the additional triplets at $\omega_1\pm 4\Omega_1$. Furthermore, as α increases still further, additional triplets will emerge at $\omega_1\pm 6\Omega_1$, $\omega_1\pm 8\Omega_1$, etc.

The numerical calculations of the fluorescence spectrum indicate that qualitatively new types of behavior arise when the atom is driven by a bichromatic field with one strong and one weak component. As expected, we have found that in this case the fluorescence spectrum is more complex than that for a monochromatic driving field. Moreover, different types of spectra are observed depending on the values of Δ_2 and α. In the next section, we present a dressed-atom calculation, which provides analytical expressions for the fluorescence spectra, and gives a physical interpretation of the appearance and disappearance of the spectral peaks, their intensities and their widths.

C. Absorption spectrum

We now introduce a third tunable probe beam of frequency ω_p and amplitude E_p, sufficiently weak that it does not appreciably perturb the atom-driving field system. The steady-state absorption spectrum of the probe field can be written in terms of the Fourier transform of the average value of the two-time commutator of the atomic operators as [25]

$$W(\omega_p)=W_0\mathrm{Re}\int_0^\infty d\tau e^{i(\omega_p-\omega_s)\tau}D(\tau), \qquad (3.19)$$

[2]In Sec. IV we will find that the intensity of the incoherent peak at ω_1 is proportional to $\Delta_2^2/(\Omega_2^2+\Delta_2^2)$ for small Δ_2. Our numerical calculations show a peak at ω_1 beginning to emerge at $\Delta_2\sim 0.2\Gamma$, having an amplitude $\sim 10\%$ that of the doublet peak amplitudes for $\Delta_2\sim\Gamma$, and $\sim 20\%$ for $\Delta_2\sim 1.6\Gamma$.

where

$$W_0 = 2\omega_p \Gamma u(\vec{r}) |\vec{\mu}\cdot\vec{E}_p|^2/\hbar, \tag{3.20}$$

and

$$D(\tau) = \lim_{t\to\infty} \langle [\tilde{S}^-(t+\tau), \tilde{S}^+(t)] \rangle. \tag{3.21}$$

Using Laplace transforms, we rewrite the absorption spectrum (3.19) in the form

$$W(\omega_p) = W_0 \mathrm{Re}\ D(z)|_{z=-i\eta}, \tag{3.22}$$

where $\eta = (\omega_p - \omega_s)/\Gamma$, and $D(z)$ is the Laplace transform of the commutator $D(\tau)$.

For the commutators

$$R_1(\tau) = \langle [\tilde{S}^-(t+\tau), \tilde{S}^+(t)] \rangle,$$

$$R_2(\tau) = \langle [\tilde{S}^+(t+\tau), \tilde{S}^+(t)] \rangle,$$

$$R_3(\tau) = \langle [S^z(t+\tau), \tilde{S}^+(t)] \rangle, \tag{3.23}$$

the optical Bloch equations (3.1) lead to the same recurrence relation as Eq. (3.6), but with the components $X_i(t)$ replaced by $R_i(\tau)$ and $\vec{X}^{(l)}(0)$ by

$$\vec{X}^{(l)}(0) \to \vec{R}^{(l)}(0) = \begin{pmatrix} -2X_3^{(l)}(t) \\ 0 \\ -X_2^{(l)}(t) \end{pmatrix}. \tag{3.24}$$

The steady-state absorption spectrum takes the form

$$W(\omega_p) = W_0 \mathrm{Re}\ R_1^{(0)}(z)|_{z=-i\eta}. \tag{3.25}$$

In Fig. 4, we plot this spectrum for $2\Omega_1 = 50\Gamma$, $\alpha = 0.1$ and different detunings Δ_1 and Δ_2. For $\Delta_1 = \Delta_2 = 0$, we observe an emission-absorption feature centered at ω_1 and emission-dispersion-absorption features centered at ω_2 and $2\omega_1 - \omega_2$. As in the fluorescence spectrum, there is no central component at ω_1. When both Δ_1 and Δ_2 differ from zero an additional dispersionlike feature develops at ω_1. Moreover, the amplitudes of the features centered near $\omega_1 + 2\Omega_1$ increase as the detunings increase, whereas the feature centered at $\omega_1 - 2\Omega_1$ is reduced to an emission line. In Fig. 5, we plot the spectrum for $\Delta_1 = \Delta_2 = 0$, with $\alpha = 0.1$ and 0.2, respectively. The spectrum is qualitatively unchanged, but the intensity of the emission and absorption lines increases linearly with α and for $\alpha = 0.2$ is double that for $\alpha = 0.1$.

It is difficult to understand the physical origin of these spectral features from the calculations described thusfar. However, in the next section we study the system and recalculate the absorption spectrum in terms of the doubly-dressed-atom model [30]. Since one of the bichromatic components is more intense than the other, this model provides a good approach for studying the problem, both qualitatively and quantitatively, and in the limit of well-separated spectral features leads to both simple analytical solutions and a transparent physical explanation.

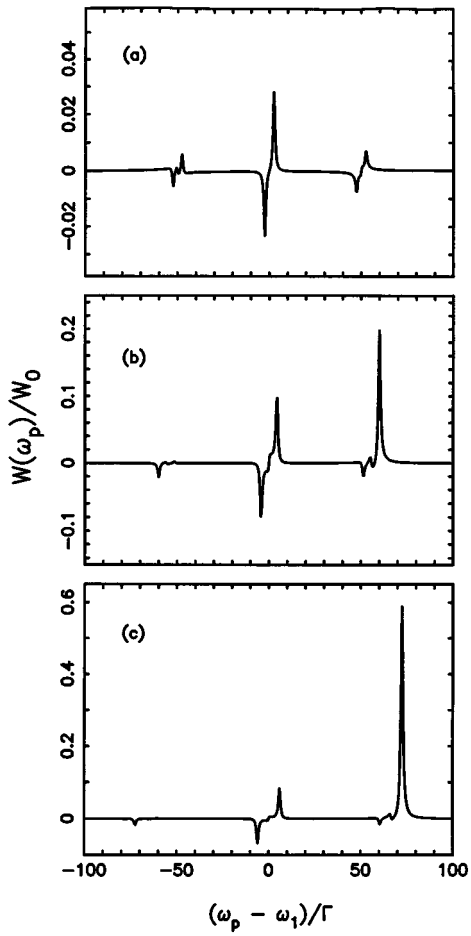

FIG. 4. The absorption spectrum for $2\Omega_1 = 50\Gamma$, $\alpha = 0.1$, and different θ, ϕ. (a) $\theta = \phi = \pi/4$, (b) $\theta = \phi = \pi/6$, (c) $\theta = \phi = \pi/8$.

IV. FLUORESCENCE AND ABSORPTION SPECTRA: A DRESSED-ATOM APPROACH

In this section we calculate analytically the fluorescence and absorption spectra of a two-level atom driven by a bichromatic field with one strong and one weak component. We treat the field quantum mechanically, and first derive the eigenstates (dressed states) of the combined system. We then

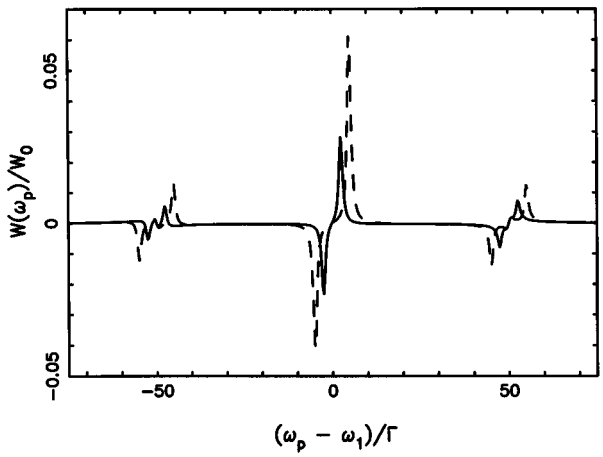

FIG. 5. The absorption spectrum for $2\Omega_1 = 50\Gamma$, $\theta = \phi = \pi/4$ and different α: $\alpha = 0.1$ (solid line), $\alpha = 0.2$ (dashed line).

use these states as basis states for further calculations. The model is valid in the limits

$$\omega_s \gg \Omega_1 > \Omega_2 > \Gamma. \tag{4.1}$$

A. Dressed states

The Hamiltonian (2.8) of the uncoupled system of atom and driving field has eigenstates $|j\rangle|N,M\rangle$ which satisfy the eigenvalue equation

$$H_0'|j\rangle|N,M\rangle = (E_j + N\hbar\omega_1 + M\hbar\omega_2)|j\rangle|N,M\rangle, \tag{4.2}$$

where E_j is the energy of the atom in state $|j\rangle$ $(j=e,g)$, and $N(M)$ is the number of photons in laser mode 1(2). We find the eigenstates of the coupled system by performing a ''double-dressing'' calculation, recently used [30] to study a system consisting of a (monochromatically) strongly driven atom coupled to a single mode of a cavity. In these calculations, we first find the eigenstates of the Hamiltonian of the atom and strong field component

$$H_{da} = \hbar\omega_0 S^z + \hbar\omega_1 a_1^+ a_1 + \hbar g_1 (a_1^+ S^- + S^+ a_1). \tag{4.3}$$

This Hamiltonian has eigenstates $|i,N\rangle$, $i=1,2$, satisfying the eigenvalue equation

$$H_{da}|i,N\rangle = \hbar[N\omega_1 - (-1)^i\Omega]|i,N\rangle, \tag{4.4}$$

where

$$|1,N\rangle = \sin\theta|g,N\rangle + \cos\theta|e,N-1\rangle,$$
$$|2,N\rangle = \cos\theta|g,N\rangle - \sin\theta|e,N-1\rangle, \tag{4.5}$$

are the (singly) dressed-atom states, with

$$\cos^2\theta = \frac{1}{2} + \frac{\Delta_1}{4\Omega}, \tag{4.6}$$

and

$$2\Omega = (4\Omega_1^2 + \Delta_1^2)^{1/2} \tag{4.7}$$

the detuned Rabi frequency of the strong component [24].

The Hamiltonian H_2 of the noninteracting singly dressed atom and weak component

$$H_2 = H_{da} + \hbar\omega_2 a_2^+ a_2 \tag{4.8}$$

has the eigenvalue equation

$$H_2|i,N,M\rangle = \hbar[N\omega_1 - (-1)^i\Omega + M\omega_2]|i,N,M\rangle, \tag{4.9}$$

where $1 \ll M \ll N$. In the following, as in Sec. III, we will assume that the frequency of the weak component is close to the Rabi sideband frequency $\omega_1 + 2\Omega$, with a detuning $\Delta_2 = \omega_1 + 2\Omega - \omega_2$.

The states $|i,N,M\rangle$, appearing in Eq. (4.9), are the ''undressed'' states of the (uncoupled) system. It is easy to show from Eq. (4.9) that these states group into manifolds each containing an infinite number of doublets [see Fig. 6(a)]. Neighboring manifolds are separated by frequency ω_1, while neighboring doublets within each manifold are separated by 2δ. The states within each doublet are separated by Δ_2.

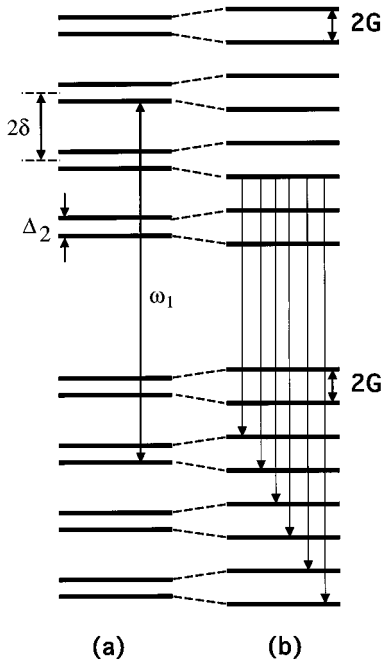

FIG. 6. Energy level diagram of the undressed system (a), and of the doubly dressed atom (b).

When we include the interaction W between the singly dressed atom and the weak field component,

$$W = \hbar g_2 (a_2^+ S^- + S^+ a_2), \tag{4.10}$$

the doublets recombine into new doublets with eigenstates

$$|N+M,n+\rangle = \sin\phi|2,N-n-1,M+n+1\rangle + \cos\phi|1,N-n,M+n\rangle,$$
$$|N+M,n-\rangle = \cos\phi|2,N-n-1,M+n+1\rangle - \sin\phi|1,N-n,M+n\rangle, \tag{4.11}$$

corresponding to energies

$$E_{N+M,n\pm} = (N+M)\omega_1 + (2M+2n+1)\Omega - (M+n)\Delta_2 \pm G, \tag{4.12}$$

where

$$\cos^2\phi = \frac{1}{2} + \frac{\Delta_2}{4G} \tag{4.13}$$

and

$$2G = (4\Omega_2^2\cos^4\theta + \Delta_2^2)^{1/2} \tag{4.14}$$

is the detuned Rabi frequency of the weak field component. Thus, the states (4.11) are (also) grouped into manifolds, each containing an infinite number of doublets [Fig. 6(b)]. Neighboring doublets are separated by 2Ω, while the intradoublet separation is $2G$.

B. Transition rates

Interaction between the atom and the vacuum modes of the electromagnetic field leads to a spontaneous emission cascade by the dressed atom down its energy manifold ladder. The probability of a transition between any two dressed states is proportional to the absolute square of the dipole transition moment connecting them [24]. It is easily verified that nonzero dipole moments occur only between states within neighboring manifolds. Using (4.11), we find that the dipole transition moments between $|N+M,n\pm\rangle$ and $|N+M-1,m\pm\rangle$ are

$$\langle n+,N+M|S^+|N+M-1,m+\rangle = \cos 2\phi \sin\theta \cos\theta \delta_{n,m} + \frac{1}{2}\sin 2\phi \cos^2\theta \delta_{n,m+1} - \frac{1}{2}\sin 2\phi \sin^2\theta \delta_{n,m-1}, \tag{4.15}$$

$$\langle n+,N+M|S^+|N+M-1,m-\rangle = -\sin^2\phi \sin\theta \cos\theta \delta_{n,m} + \cos^2\phi \cos^2\theta \delta_{n,m+1} + \sin^2\phi \sin^2\theta \delta_{n,m-1}, \tag{4.16}$$

$$\langle n-,N+M|S^+|N+M-1,m+\rangle = -\sin 2\phi \sin\theta \cos\theta \delta_{n,m} - \sin^2\phi \cos^2\theta \delta_{n,m+1} - \cos^2\phi \sin^2\theta \delta_{n,m-1}, \tag{4.17}$$

$$\langle n-,N+M|S^+|N+M-1,m-\rangle = -\cos 2\phi \sin\theta \cos\theta \delta_{n,m} - \frac{1}{2}\sin 2\phi \cos^2\theta \delta_{n,m+1} + \frac{1}{2}\sin 2\phi \sin^2\theta \delta_{n,m-1}. \tag{4.18}$$

The presence of the δ functions in Eqs. (4.15)–(4.18) indicates that from a given doublet $|N+M,n\pm\rangle$ spontaneous emission can occur to doublets $|N+M-1,m\pm\rangle$ with $m=n,n\pm1$ only. These transitions occur with probabilities

$$\Gamma_{ni,mj} = \Gamma |\langle ni,N+M|S^+|N+M-1,mj\rangle|^2 \tag{4.19}$$

at (nine different) frequencies

$$\omega_{ni,mj} = \hbar^{-1}(E_{N+M,ni} - E_{N+M-1,mj}), \tag{4.20}$$

given by the expressions

$$\Gamma_{n\pm,n\pm} = \Gamma \cos^2 2\phi \sin^2\theta \cos^2\theta, \quad \omega_{n\pm,n\pm} = \omega_1,$$

$$\Gamma_{n\pm,n\mp} = \Gamma \sin^2 2\phi \sin^2\theta \cos^2\theta, \quad \omega_{n\pm,n\mp} = \omega_1 \pm 2G,$$

$$\Gamma_{n\pm,(n-1)\pm} = \frac{1}{4}\Gamma \sin^2 2\phi \cos^4\theta, \quad \omega_{n\pm,(n-1)\pm} = \omega_2,$$

$$\Gamma_{n\pm,(n+1)\pm} = \frac{1}{4}\Gamma \sin^2 2\phi \sin^4\theta, \quad \omega_{n\pm,(n+1)\pm} = 2\omega_1 - \omega_2,$$

$$\Gamma_{n+,(n-1)-} = \Gamma \cos^4\phi \cos^4\theta, \quad \omega_{n+,(n-1)-} = \omega_2 + 2G,$$

$$\Gamma_{n+,(n+1)-} = \Gamma \sin^4\phi \sin^4\theta,$$

$$\omega_{n+,(n+1)-} = 2\omega_1 - \omega_2 + 2G,$$

$$\Gamma_{n-,(n-1)+} = \Gamma \sin^4\phi \cos^4\theta, \quad \omega_{n-,(n-1)+} = \omega_2 - 2G,$$

$$\Gamma_{n-,(n+1)+} = \Gamma \cos^4\phi \sin^4\theta,$$

$$\omega_{n-,(n+1)+} = 2\omega_1 - \omega_2 - 2G. \tag{4.21}$$

The total spontaneous emission decay rates from $|N+M,n\pm\rangle$ are then given by

$$\Gamma_{n+} = \sum_{mj} \Gamma_{n+,mj} = \Gamma(\cos^2\theta \cos^2\phi + \sin^2\theta \sin^2\phi), \tag{4.22}$$

$$\Gamma_{n-} = \sum_{mj} \Gamma_{n-,mj} = \Gamma(\sin^2\theta \cos^2\phi + \cos^2\theta \sin^2\phi). \tag{4.23}$$

From the transition rates of Eq. (4.21), it is apparent that the spectrum contains nine lines for general values of ϕ and θ. If we keep the strong driving component nearly resonant with the atom ($\omega_1 \approx \omega_0$ or $\theta \approx \pi/4$), the number of lines will vary with the detuning of the weak component. For example, for $\phi=\pi/4$ ($\Delta_2=0$), the transition rates $\Gamma_{n\pm,n\pm}$ vanish, the spectral line at ω_1 disappears, and eight lines remain in the spectrum; this case is plotted in Figs. 2(c) and 7(c). Similarly, for large Δ_2, $\sin^2\phi$, $\sin^2 2\phi \to 0$. The number of spectral lines is then reduced to three, at $\omega_1, \omega_2+2G \approx \omega_1+2(\Omega+\delta)$, and $2\omega_1-\omega_2-2G \approx \omega_1-2(\Omega+\delta)$, very similar to the Mollow triplet [Figs. 2(a) and 7(a)]. The spectra will be discussed in detail in Sec. IV E.

C. Populations of the dressed states

To study the evolution of the populations of the dressed states, we project the master equation (2.2) onto $|N+M,n\pm\rangle$ on the right and $\langle n\pm,N+M|$ on the left. We make the secular approximation (ignoring nonsecular couplings between populations and coherences), denote the populations of states $|N+M,n\pm\rangle$ by $\Pi_{n\pm}^{N+M}$,

$$\Pi_{n\pm}^{N+M} \equiv \langle n\pm,N+M|\rho|N+M,n\pm\rangle, \tag{4.24}$$

and introduce the ''reduced'' populations $\Pi_n^{\pm} = \Sigma_{N,M}\Pi_{n\pm}^{N+M}$ [24]. The equations of motion of $\Pi_n^{\pm}(\tau)$ can be written in the form

$$\frac{d}{d\tau}\Pi_n^+(\tau)=-\left(\frac{1}{4}\sin^2 2\phi\,\sin^2 2\theta+\cos^2\phi\,\cos^4\theta+\sin^2\phi\,\sin^4\theta\right)\Pi_n^+(\tau)+\frac{1}{4}\sin^2 2\phi\,\sin^2 2\theta\Pi_n^-(\tau)$$
$$+\sin^2\phi\,\cos^4\theta[\cos^2\phi\Pi_{n+1}^+(\tau)+\sin^2\phi\Pi_{n+1}^-(\tau)]+\cos^2\phi\,\sin^4\theta[\sin^2\phi\Pi_{n-1}^+(\tau)+\cos^2\phi\Pi_{n-1}^-(\tau)], \tag{4.25}$$

$$\frac{d}{d\tau}\Pi_n^-(\tau)=-\left(\frac{1}{4}\sin^2 2\phi\,\sin^2 2\theta+\sin^2\phi\,\cos^4\theta+\cos^2\phi\,\sin^4\theta\right)\Pi_n^-(\tau)+\frac{1}{4}\sin^2 2\phi\,\sin^2 2\theta\Pi_n^+(\tau)$$
$$+\cos^2\phi\,\cos^4\theta[\cos^2\phi\Pi_{n+1}^+(\tau)+\sin^2\phi\Pi_{n+1}^-(\tau)]+\sin^2\phi\,\sin^4\theta[\sin^2\phi\Pi_{n-1}^+(\tau)+\cos^2\phi\Pi_{n-1}^-(\tau)], \tag{4.26}$$

where $\tau=\Gamma t$. Because $M\gg 1$, as in the case of monochromatic driving [24] we can assume that the populations vary slowly with n, and write

$$\Pi_n^+=\Pi_{n\pm1}^+=\cdots=\Pi^+,$$
$$\Pi_n^-=\Pi_{n\pm1}^-=\cdots=\Pi^-. \tag{4.27}$$

Equations (4.25) and (4.26) then reduce to a set of two coupled equations, which in the steady-state ($\tau\to\infty$) has the solution:

$$\frac{\Pi^+}{\Pi^-}=\frac{\frac{1}{4}\sin^2 2\phi\,\sin^2 2\theta+\sin^4\phi\,\cos^4\theta+\cos^4\phi\,\sin^4\theta}{\frac{1}{4}\sin^2 2\phi\,\sin^2 2\theta+\sin^4\phi\,\sin^4\theta+\cos^4\phi\,\cos^4\theta}. \tag{4.28}$$

It is evident from Eq. (4.28) that for general ϕ,θ the dressed states are unequally populated. However, it is easily verified that when either $\phi=\pi/4$ or $\theta=\pi/4$, the population is equally distributed, and $\Pi^+=\Pi^-$.

D. Coherences and spectral linewidths

The fluorescence spectrum is related to the time evolution of the atomic dipole moment operator S^+ [24]

$$S^+=\sum_{\substack{ni,mj\\N,M}} S_{ni,mj}^+\rho_{ni,mj,N,M}^{(+)}, \tag{4.29}$$

where $S_{ni,mj}^+=\langle ni,N+M|S^+|N+M-1,mj\rangle$ are given by Eqs. (4.15)–(4.18), and $\rho_{ni,mj,N,M}^{(+)}$ are the coherences

$$\rho_{ni,mj,N,M}^{(+)}=|N+M,ni\rangle\langle mj,N+M-1|, \tag{4.30}$$

which are off-diagonal elements of the density matrix, and oscillate at frequencies (4.21).

First, we consider the transitions at $\omega_1\pm 2G$, $\omega_2\pm 2G$, and $2\omega_1-\omega_2\pm 2G$. For values of Ω and G corresponding to the range (4.1), it is easily verified that the spectral lines are all nonoverlapping. The equations of motion of the corresponding density matrix elements are therefore uncoupled and from the master equation (2.2) we find that they are given by

$$\dot\rho_{ni,mj,N,M}^{(+)}=-(i\omega_{ni,mj}+\Gamma_c)\rho_{ni,mj,N,M}^{(+)}, \tag{4.31}$$

where $\omega_{ni,mj}=\omega_1\pm 2G,\omega_2\pm 2G,2\omega_1-\omega_2\pm 2G$ are the frequencies of the spectral lines, and

$$\Gamma_c=\frac{1}{4}\Gamma[2+\sin^2 2\phi(\cos^4\theta+\sin^4\theta)+\cos^2 2\phi\,\sin^2 2\theta], \tag{4.32}$$

is their linewidth.

For the central component of the spectrum, the two matrix elements $\rho_{n+,n+,N,M}^{(+)}$ and $\rho_{n-,n-,N,M}^{(+)}$ oscillate at the same frequency ω_1, and therefore have coupled equations of evolution. When we average over the driving field, the reduced coherences $\rho_{n\pm,n\pm}^{(+)}=\Sigma_{NM}\rho_{n\pm,n\pm,N,M}^{(+)}$ are found to obey the same coupled equations of motion as do the populations $\Pi^\pm$, with the addition in each of the freely oscillating term $-i\omega_1\rho_{n\pm,n\pm}^{(+)}$, and are given by

$$\dot\rho_{n+,n+}^{(+)}(t)=-(i\omega_1+A)\rho_{n+,n+}^{(+)}(t)+B\rho_{n-,n-}^{(+)}(t),$$
$$\dot\rho_{n-,n-}^{(+)}(t)=-(i\omega_1+B)\rho_{n-,n-}^{(+)}(t)+A\rho_{n+,n+}^{(+)}(t), \tag{4.33}$$

where

$$A=\left(\frac{1}{4}\sin^2 2\phi\,\sin^2 2\theta+\cos^4\phi\,\cos^4\theta+\sin^4\phi\,\sin^4\theta\right)\Gamma, \tag{4.34}$$

$$B=\left(\frac{1}{4}\sin^2 2\phi\,\sin^2 2\theta+\sin^4\phi\,\cos^4\theta+\cos^4\phi\,\sin^4\theta\right)\Gamma. \tag{4.35}$$

The associated dipole moments $p_{n\pm,n\pm}^{(+)}=S_{n\pm,n\pm}^+\rho_{n\pm,n\pm}^{(+)}$ then obey the equations

$$\dot p_{n+,n+}^{(+)}(t)=-(i\omega_1+A)p_{n+,n+}^{(+)}(t)-Bp_{n-,n-}^{(+)}(t),$$
$$\dot p_{n-,n-}^{(+)}(t)=-(i\omega_1+B)p_{n-,n-}^{(+)}(t)-Ap_{n+,n+}^{(+)}(t), \tag{4.36}$$

whose solutions are readily found to be

$$\begin{pmatrix} p^{(+)}_{n+,n+}(t) \\ p^{(+)}_{n-,n-}(t) \end{pmatrix} = \frac{a_1}{\sqrt{A^2+B^2}} \begin{pmatrix} B \\ -A \end{pmatrix} e^{-i\omega_1 t} + a_2 \begin{pmatrix} 1 \\ 1 \end{pmatrix} e^{-(i\omega_1+\Gamma_p)t}, \tag{4.37}$$

where the constants a_1 and a_2 can be found from initial conditions. We do not, however, require the values of a_1 and a_2 in order to calculate the fluorescence spectrum and therefore do not solve for them. The first term in Eq. (4.37) corresponds to the elastic component, while the second term corresponds to the inelastic central component at frequency ω_1 with linewidth given by

$$\Gamma_p = A+B = \Gamma\left[\frac{1}{2}\sin^2 2\phi \sin^2 2\theta + (\sin^4\phi+\cos^4\phi)(\sin^4\theta+\cos^4\theta)\right]. \tag{4.38}$$

Finally, we consider the evolution of the off-diagonal elements $p^{(+)}_{n+,(n\pm1)+}$, which are related to the components at frequencies $2\omega_1-\omega_2$ and ω_2. These elements are coupled to the matrix elements $p^{(+)}_{n-,(n\pm1)-}$, which oscillate at the same frequencies. It is easily verified that the dipole moments associated with these elements obey the same equations of motion as (4.33), but with ω_1 replaced by $2\omega_1-\omega_2$ for the elements $p^{(+)}_{n\pm,(n+1)\pm}$ and by ω_2 for the elements $p^{(+)}_{n\pm,(n-1)\pm}$. Their solutions are the same as given in Eq. (4.37) and their linewidths the same as that of the central component at ω_1 [Eq. (4.38)].

E. Fluorescence spectrum

The fluorescence spectrum is given by the real part of the Fourier transform of the correlation function of the dipole-moment operator $\langle p^{(+)}(t)p^{(-)}(t')\rangle$, $t>t'$. From the quantum regression theorem [29], it is well known that for $t>t'$ the two-time average $\langle p^{(+)}_{ni,mj}(t)p^{(-)}(t')\rangle$ satisfies the same equation of motion as the one-time average $\langle p^{(+)}_{ni,mj}(t)\rangle$, with the initial conditions

$$\langle p^{(+)}_{ni,mj}(t')p^{(-)}(t')\rangle = \Gamma_{ni,mj}\Pi^i, \tag{4.39}$$

where $\Gamma_{ni,mj}$ are given by Eq. (4.21), and Π^i are the steady-state populations of the dressed states given by Eq. (4.28). The equations of motion for the one-time averages $\langle p^{(+)}_{ni,mj}(t)\rangle$ were obtained in Sec. IV D. Thus, in the limit of large $G(G>\Gamma)$, where the spectral lines do not overlap, the fluorescence spectrum is given by

$$\begin{aligned} S_{in}(\omega) = u(\vec{r})\Bigg\{ & \frac{(\Gamma_{n+,n+}\Pi^+ + \Gamma_{n-,n-}\Pi^-)\Gamma_p}{(\omega-\omega_1)^2+\Gamma_p^2} + \frac{(\Gamma_{n+,(n+1)+}\Pi^+ + \Gamma_{n-,(n+1)-}\Pi^-)\Gamma_p}{(\omega-2\omega_1+\omega_2)^2+\Gamma_p^2} \\ & + \frac{(\Gamma_{n+,(n-1)+}\Pi^+ + \Gamma_{n-,(n-1)-}\Pi^-)\Gamma_p}{(\omega-\omega_2)^2+\Gamma_p^2} + \frac{\Gamma_{n+,n-}\Pi^+\Gamma_c}{(\omega-\omega_1-2G)^2+\Gamma_c^2} + \frac{\Gamma_{n-,n+}\Pi^-\Gamma_c}{(\omega-\omega_1+2G)^2+\Gamma_c^2} + \frac{\Gamma_{n+,(n-1)-}\Pi^+\Gamma_c}{(\omega-\omega_2-2G)^2+\Gamma_c^2} \\ & + \frac{\Gamma_{n-,(n-1)+}\Pi^-\Gamma_c}{(\omega-\omega_2+2G)^2+\Gamma_c^2} + \frac{\Gamma_{n+,(n+1)-}\Pi^+\Gamma_c}{(\omega-2\omega_1+\omega_2-2G)^2+\Gamma_c^2} + \frac{\Gamma_{n-,(n+1)+}\Pi^-\Gamma_c}{(\omega-2\omega_1+\omega_2+2G)^2+\Gamma_c^2}\Bigg\}. \end{aligned} \tag{4.40}$$

In Fig. 7, we plot the analytical expression (4.40) for the incoherent part[3] of the fluorescence spectrum for the same parameters as in Fig. 2, where we have plotted the spectrum calculated numerically. It is seen that the positions of the spectral lines, their linewidths and intensities calculated from the analytical expression (4.40) are in good agreement with the numerical results.

Having available the analytical solution for the fluorescence spectrum, it is easy to explain its strong dependence on the detuning Δ_2, which is seen in Figs. 2 and 7. For large Δ_2 [Figs. 2(a) and 7(a)], $\sin^2\phi\to 0$ and most of the transition rates $\Gamma_{ni,mj}$ vanish, except for $\Gamma_{n\pm,n\pm}$, $\Gamma_{n+,(n-1)-}$, and $\Gamma_{n-,(n+1)+}$. In this limit the spectrum reduces to the familiar Mollow triplet [1]. As Δ_2 decreases [Figs. 2(b) and 7(b)], $\sin\phi$ increases somewhat, which results in nonzero transition rates $\Gamma_{n\pm,n\pm}$, $\Gamma_{n\pm,(n+1)\pm}$, $\Gamma_{n\pm,n\mp}$, and $\Gamma_{n\pm,(n-1)\pm}$; the remaining rates $\Gamma_{n+,(n+1)-}$ and $\Gamma_{n-,(n-1)+}$ are proportional to $\sin^4\phi$ and still very small. In this case the spectrum exhibits three lines near the central component and two lines near each Rabi sideband. When $\Delta_2\equiv 0$, $\phi=\pi/4$ and all transition rates are different from zero except for $\Gamma_{n\pm,n\pm}$, causing the central component at ω_1 to disappear, as seen in Figs. 2(c) and 7(c).

For high α, the numerical calculation of the fluorescence spectrum [Fig. 3(c)] predicts additional triplet structures located near $\omega_1\pm 4\Omega$. Moreover, these calculations predict the reappearance of the central component at ω_1 even when $\theta=\phi=\pi/4$. The analytical expression (4.40), however, predicts neither the additional triplet structures nor the reappearance of the central component. In order to explain these features analytically, we have to go beyond the zero-order approximation in α in the calculation of the dressed states. We have thus far neglected the coupling via W of the states $|N+M,n\pm\rangle$ to the states $|N+M,(n\pm1)\pm\rangle$ and $|N+M,(n\pm2)\pm\rangle$. This coupling is of order $\hbar G$, while the states are separated from $|N+M,n\pm\rangle$ in energy by amounts of order $\hbar\Omega$, so that the coupling introduces correction terms into the dressed states of order $G/\Omega\approx\alpha$. Here, we include this coupling and calculate the first-order corrections to the states.

From Eq. (4.11), we find that the states $|N+M,n\pm\rangle$ are

[3]The coherent part of the spectrum vanishes for the parameters chosen ($\omega_1=\omega_0$ or $\theta=\pi/4$).

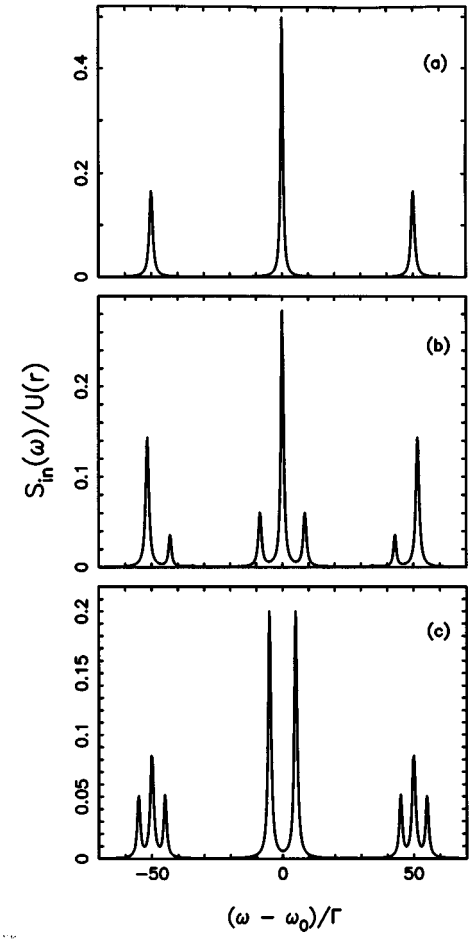

FIG. 7. The fluorescence spectrum plotted from the analytical expression, Eq. (4.40), for $\omega_1=\omega_0$, $2\Omega_1=50\Gamma$, $\alpha=0.2$ and different Δ_2: (a) $\Delta_2 \gg 50\Gamma$, (b) $\Delta_2=7\Gamma$, (c) $\Delta_2=0$.

coupled to the states $|N+M,(n\pm1)\pm\rangle$ and $|N+M,(n\pm2)\pm\rangle$ with the following nonzero matrix elements:

$$\begin{aligned}
&\langle N+M,(n\pm1)-|W|N+M,n+\rangle \\
&\quad=\langle N+M,(n\pm1)+|W|N+M,n-\rangle \\
&\quad=-G, \\
&\langle N+M,(n-2)\pm|W|N+M,n+\rangle \\
&\quad=\langle N+M,(n+2)+|W|N+M,n\pm\rangle \\
&\quad=-\tfrac{1}{2}G, \\
&\langle N+M,(n-2)\pm|W|N+M,n-\rangle \\
&\quad=\langle N+M,(n+2)-|W|N+M,n\pm\rangle \\
&\quad=\tfrac{1}{2}G, \qquad (4.41)
\end{aligned}$$

where, for simplicity, we have assumed that $\theta=\phi=\pi/4$. Using first-order perturbation theory, we find the states $|N+M,n\pm\rangle$ correct to first order in α to be

$$\begin{aligned}
|N+M,n+\rangle^{(1)}=&|N+M,n+\rangle+\frac{\alpha}{2}[|N+M,(n+1)-\rangle \\
&-|N+M,(n-1)-\rangle] \\
&-\frac{\alpha}{8}[|N+M,(n-2)-\rangle \\
&+|N+M,(n-2)+\rangle-|N+M,(n+2)+\rangle \\
&+|N+M,(n+2)-\rangle], \qquad (4.42)
\end{aligned}$$

$$\begin{aligned}
|N+M,n-\rangle^{(1)}=&|N+M,n-\rangle+\frac{\alpha}{2}[|N+M,(n+1)+\rangle \\
&-|N+M,(n-1)+\rangle] \\
&+\frac{\alpha}{8}[|N+M,(n-2)-\rangle \\
&+|N+M,(n-2)+\rangle+|N+M,(n+2)+\rangle \\
&-|N+M,(n+2)-\rangle]. \qquad (4.43)
\end{aligned}$$

Using the above corrections to the dressed states, we find that additional transitions are predicted at the frequencies $\omega_1\pm4(\Omega-\frac{1}{2}\Delta_2)$ and $\omega_1\pm4(\Omega-\frac{1}{2}\Delta_2)\pm2G$ with probability

$$\Gamma_{n\pm,(n+2)\pm}=\Gamma_{n\pm,(n-2)\pm}=\Gamma_{n\pm,(n+2)\mp}=\Gamma_{n\pm,(n-2)\mp}=\frac{\alpha^2\Gamma}{64}. \qquad (4.44)$$

Thus, the additional triplet structures in the spectrum in the vicinity of $\omega_1\pm4\Omega$ occur with intensities proportional to $\alpha^2/64$, and appear only for high α.

In a similar way, it is straightforward to show that for $\theta=\phi=\pi/4$ transitions at the central frequency ω_1 occur with probability

$$\Gamma^{(1)}_{n\pm,n\pm}=\frac{\alpha^4\Gamma}{16}, \qquad (4.45)$$

which is two orders in α smaller than those of the additional triplet structures at $\omega_1\pm4\Omega$. Thus the central component reappears only for relatively larger values of α than those at which the additional triplet structures become visible. In a similar way too, by including in our calculations terms involving successively higher powers of α, we predict the appearance of additional triplets in the spectrum centered at frequencies $\omega_1\pm2n\Omega$, $n\geqslant1$, with intensities proportional to $\alpha^{2(n-1)}$.

F. Absorption spectrum

According to Eq. (3.19), the absorption spectrum of a weak probe beam is given by the real part of the Fourier transform of the commutator $\langle[S^-(t),S^+(t')]\rangle$, the first term of which is associated with absorption and the second with stimulated emission by the system. From the quantum regression theorem [29], it is well known that for $t>t'$ the two-time commutator $\langle[S^-_{ni,mj}(t),S^+(t')]\rangle$ satisfies the same equation of motion as does the density matrix element

$[\rho^{(+)}_{ni,mj}(t)]^*$, with the initial condition

$$\langle [S^-_{ni,mj}(t'),S^+(t')]\rangle = \Gamma_{ni,mj}(\Pi^i-\Pi^j). \tag{4.46}$$

Thus, it is straightforward to show that in the case of nonoverlapping spectral components, the absorption spectrum of a probe beam is given by

$$W(\omega_p) = W_0\left\{ \frac{\Gamma_{n-,n+}(\Pi^+-\Pi^-)\Gamma_c}{(\omega_p-\omega_1+2G)^2+\Gamma_c^2} + \frac{\Gamma_{n+,n-}(\Pi^--\Pi^+)\Gamma_c}{(\omega_p-\omega_1-2G)^2+\Gamma_c^2} + \frac{\Gamma_{n+,(n-1)-}(\Pi^--\Pi^+)\Gamma_c}{(\omega_p-\omega_2-2G)^2+\Gamma_c^2} + \frac{\Gamma_{n-,(n-1)+}(\Pi^+-\Pi^-)\Gamma_c}{(\omega_p-\omega_2+2G)^2+\Gamma_c^2} \right.$$
$$\left. + \frac{\Gamma_{n+,(n+1)-}(\Pi^--\Pi^+)\Gamma_c}{(\omega_p-2\omega_1+\omega_2-2G)^2+\Gamma_c^2} + \frac{\Gamma_{n-,(n+1)+}(\Pi^+-\Pi^-)\Gamma_c}{(\omega_p-2\omega_1+\omega_2+2G)^2+\Gamma_c^2} \right\}. \tag{4.47}$$

It is easily verified that the components of the absorption spectrum have the same positions and linewidths as their counterparts in the fluorescence spectrum but that they have widely differing intensities. The net absorption at any frequency is proportional to the transition rate $\Gamma_{ni,mj}$ and the difference between the populations of the lower and upper levels in the transition. In Figs. 4(b) and 4(c), we plot the absorption spectrum for $\theta=\phi\neq\pi/4$, corresponding to populations $\Pi^->\Pi^+$. In Fig. 4(a), we plot the spectrum for $\theta=\phi=\pi/4$, and hence, according to Eq. (4.28), for equal $\Pi^\pm$. Yet, in this case too, amplification lines appear at ω_1-2G, ω_2-2G, and $2\omega_1-\omega_2-2G$, and absorption lines at their corresponding $+2G$ counterparts, indicating that $\Pi^->\Pi^+$ in Fig. 4(a) as well. In order to explain these features, it is necessary to go beyond the zero-order in α expressions (4.28) for the steady-state populations.

In Eqs. (4.42) and (4.43), we obtained expressions for the eigenstates $|N+M,n\pm\rangle$ correct to first order in α. If we use these corrected eigenstates to study the evolution of the populations, as in Sec. IV C, for $\theta=\phi=\pi/4$ we obtain for $\Pi^\pm$ the coupled equations

$$\dot{\Pi}^+ = -\frac{3\Gamma}{8}\Pi^+ + \Gamma\left(\frac{3}{8}-\frac{\alpha}{2}\right)\Pi^-,$$

$$\dot{\Pi}^- = -\frac{3\Gamma}{8}\Pi^- + \Gamma\left(\frac{3}{8}+\frac{\alpha}{2}\right)\Pi^+, \tag{4.48}$$

with the steady-state solutions

$$\Pi^\pm = \frac{3}{6\pm 4\alpha}. \tag{4.49}$$

Thus the population difference to first order in α is

$$\Pi^- - \Pi^+ = \frac{2\alpha}{3}, \tag{4.50}$$

giving rise to the nonvanishing spectral lines of Figs. 4(a). Moreover, it is evident from Eqs. (4.47) and (4.50) that the intensities for $\alpha=0.2$ are double those for $\alpha=0.1$, in agreement with the spectrum shown in Fig. 5.

V. SUMMARY

We have studied the fluorescence and absorption spectra of a two-level atom driven by a bichromatic field composed of one strong and one weak frequency component. The spectra have been found to be a sensitive function of the detuning of the weak component from a Rabi sideband induced by the strong component of the driving field. For small α, the fluorescence spectrum consists in general of nine lines. For large Δ_2, however, the spectrum reduces to the Mollow triplet at ω_1 and $\omega_1\pm 2\Omega$; for smaller (but nonzero) Δ_2 it can exhibit a triplet structure near ω_1 and doublets near the sideband frequencies. In contrast, when $\Delta_2=0$ the fluorescence spectrum exhibits a doublet structure near ω_1 and triplets near $\omega_1\pm 2\Omega$, with no fluorescence at ω_1. For larger values of α, additional triplet structures appear at frequencies $\omega_1\pm 2n\Omega (n>1)$ with intensities proportional to $\alpha^{2(n-1)}$, and the central component reemerges even for $\Delta_1=\Delta_2=0$, with an intensity proportional to α^4. All these features are explained by using the dressed-atom model of Cohen-Tannoudji and Reynaud [24], adapted to the case of a bichromatic driving field. The dressed states have been identified, and the spectral features interpreted in terms of transitions among these dressed states. We have found that the appearance and vanishing of the spectral lines for some values of Δ_2 and α is related to the vanishing of the transition rates between the corresponding dressed states.

We have also calculated the absorption spectrum of a weak probe beam monitoring the bichromatically driven two-level atom. The absorption spectrum too is a sensitive function of Δ_2, and novel spectral features are observed, consisting of absorption and emission lines located near ω_1 and $\omega_1\pm 2n\Omega$. Again, we have explained these features in terms of the dressed-atom model, and found that the emission-absorption features are related to the unequal populations of the dressed states, which are calculated as a function of α. The dressed-atom model both allows a physical interpretation of all the spectral features and gives good quantitative agreement with the full numerical calculations.

ACKNOWLEDGMENTS

This research was supported in part by the University of Queensland Travel Awards for International Collaborative Research and the Natural Sciences and Engineering Research Council of Canada, to which the authors extend thanks.

[1] B. R. Mollow, Phys. Rev. **188**, 1969 (1969).
[2] F. Schuda, C. R. Stroud, Jr., and M. Hercher, J. Phys. B **7**, L198 (1974); F. Y. Wu, R. E. Grove, and S. Ezekiel, Phys. Rev. Lett. **35**, 1426 (1975).
[3] A. M. Bonch-Bruevich, T. A. Vartanyan and N. A. Chigiev, Zh. Eskp. Teor. Fiz. **77**, 1899 (1979) [Sov. Phys. JETP **50**, 901 (1979)].
[4] G. S. Agarwal and N. Nayak, J. Opt. Soc. Am. B **1**, 164 (1984).
[5] G. Y. Kryuchkov, Opt. Commun. **54**, 19 (1985).
[6] G. S. Agarwal and N. Nayak, Phys. Rev. A **33**, 391 (1986).
[7] H. Friedmann and A. D. Wilson-Gordon, Phys. Rev. A **36**, 1336 (1987).
[8] J. H. Eberly and V. D. Popov, Phys. Rev. A **37**, 2012 (1988).
[9] W. M. Ruyten, J. Opt. Soc. Am. B **6**, 1796 (1989); Phys. Rev. A **40**, 1447 (1989); J. Opt. Soc. Am. B **9**, 1892 (1992).
[10] S. Papademetriou, S. M. Chakmakjian, and C. R. Stroud, Jr., J. Opt. Soc. Am. B **9**, 1182 (1992).
[11] S. P. Tewari and M. K. Kumari, Phys. Rev. A **41**, 5273 (1990).
[12] H. S. Freedhoff and Z. Chen, Phys. Rev. A **41**, 6013 (1990); **46**, 7328 (E) (1992).
[13] Y. Zhu, Q. Wu, A. Lezama, D. J. Gauthier, and T. Mossberg, Phys. Rev. A **41**, 6574 (1990).
[14] G. S. Agarwal, Y. Zhu, D. J. Gauthier, and T. Mossberg, J. Opt. Soc. Am. B **8**, 1163 (1991).
[15] G. S. Agarwal and Y. Zhu, Phys. Rev. A **46**, 479 (1992).
[16] Z. Ficek and H. S. Freedhoff, Phys. Rev. A **48**, 3092 (1993).
[17] Q. Wu, D. J. Gauthier, and T. W. Mossberg, Phys. Rev. A **49**, R1519 (1994).
[18] M. Elk and P. Lambropoulos, Phys. Rev. A **50**, 1490 (1994).
[19] W. Lange, H. Walther, and G. S. Agarwal, Phys. Rev. A **50**, R3593 (1994).
[20] C. Wei, Ph.D. thesis, The Australian National University, 1994.
[21] G. S. Agarwal, W. Lange, and H. Walther, Phys. Rev. A **51**, 721 (1995).
[22] S. Papademetriou, M. F. Van Leeuwen, and C. R. Stroud, Jr., Phys. Rev. A **53**, 997 (1996).
[23] C. Cohen-Tannoudji and S. Reynaud, J. Phys. B **10**, 345 (1977).
[24] C. Cohen-Tannoudji, J. Dupont-Roc, and G. Grynberg, *Atom-Photon Interactions* (Wiley, New York, 1992).
[25] B. R. Mollow, Phys. Rev. A **5**, 2217 (1972).
[26] S. M. Autler and C. M. Townes, Phys. Rev. **100**, 703 (1955).
[27] G. S. Agarwal, in *Quantum Optics*, edited by G. Höhler, Springer Tracts in Modern Physics Vol. 70 (Springer, Berlin, 1974).
[28] H. Risken, *The Fokker-Planck Equation* (Springer-Verlag, Berlin, 1984), Chap. 9.
[29] M. Lax, Phys. Rev. **172**, 350 (1968).
[30] H. Freedhoff and T. Quang, J. Opt. Soc. Am. B **10**, 1337 (1993); Phys. Rev. Lett. **72**, 474 (1994); J. Opt. Soc. Am. B **12**, 9 (1995).
[31] H. J. Kimble and L. Mandel, Phys. Rev. A **13**, 2123 (1976).
[32] N. Lu and P. R. Berman, Phys. Rev. A **36**, 3845 (1987).